RSC Advances

PAPER

View Article Online
View Journal | View Issue

Cite this: *RSC Adv.*, 2024, **14**, 3289

A highly sensitive triazole-based perfectly water soluble novel bis-Schiff base reversible fluorescent-colorimetric chemosensor for fast detection of Pb^{2+} ions†

Vanshika Sharma, Sandhya Savita and Goutam Kumar Patra *

Received 11th September 2023
Accepted 4th January 2024

DOI: 10.1039/d3ra06185j

rsc.li/rsc-advances

A reversible fluorescent-colorimetric azino bis-Schiff base receptor for the detection of Pb^{2+} in aqueous medium has been developed for the first time. Receptor **L** exhibits an excellent selective and rapid fluorescent-colorimetric response towards Pb^{2+}. The sensitivity of the fluorescent-based assay (0.53 nM) and colorimetric assay (1.0 nM) for Pb^{2+} is sufficiently good in comparison to previously reported literature. From ^{1}H NMR data, Job plot measurement and the ESI-MS spectrum, a 1 : 2 stoichiometric complexation between **L** and Pb^{2+} has been established. Receptor **L** shows a remarkable detection ability in a wide pH range of 4–8 and it has been successfully utilised in the determination of Pb^{2+} in aqueous solution of bovine serum albumin protein and in real samples. The geometry of **L** has been optimized by both DFT studies and NMR, FTIR and mass spectra. Moreover, we have studied molecular docking of the probe **L**.

1. Introduction

Many metal ions play important roles in regulation and maintenance of living organisms. Some metals are hazardous in nature, and intake of these has an adverse toxic effect on the body. Detection and removal of these types of toxic harmful elements are most essential nowadays. In the modern era, many techniques are available for the detection of heavy and harmful elements. These techniques include cold vapor atomic absorption spectrometry, inductively coupled plasma mass spectrometry, electrochemical sensing and many other recognition methods such as atomic absorption, potentiometry and ion-exchange chromatography.[1–5] These traditional methods have good selectivity and sensitivity but have some drawbacks, like being expensive and involving complicated and lengthy processes while also requiring skilled personnel, sophisticated instrumentation, high operating expenditures and difficult sample preparation processes. In order to overcome these types of issues, simple and inexpensive chemosensors that can detect analytes online in real time with little time commitment are favoured to address these problems. One of the most considered and in-demand techniques is based on optical sensing. Due to their widespread usage in the identification and monitoring of cations and anions, particularly those of a dangerous nature, colorimetric and fluorometric sensors with a "naked eye" sensing capability have recently gained popularity in the chemical, environmental, and biological fields.[6–10]

Pb^{2+} serves as a crucial transitional component and is crucial in many fields. According to the history of lead, lead nitrate manufacture for commercial purposes started in the 19th century. In the industrial domain, it was primarily used at the time as the main raw material for the creation of pigments.[11,12] Due to titanium dioxide's less hazardous effects than lead, the use of lead gradually declined over time. It did, however, significantly contribute to industrial production. It was employed in industry as a heat stabiliser in the coatings of nylon, polyester, and thermal imaging paper.[13] Recent studies claim that lead (Pb) and its compounds impair the kidney, brain system, digestive system, and other organs and systems in the body after entering through wastewater and waste residues.[14] Neurasthenia syndrome, peripheral neuropathy, and lead poisoning encephalopathy are the predominant neurological symptoms. According to WHO, the maximum contaminant level of Pb^{2+} ions in drinking water is set to 10 mg L^{-1}.[12] For this reason, much effort has been made to develop effective methods for Pb^{2+} detection. The ability of many fluorescence chemosensors to distinguish between Pb^{2+}/Ag^{+}, $Pb^{2+}/Fe^{3+}/Hg^{2+}$, and $Pb^{2+}/Hg^{2+}/Cd^{2+}$ has been demonstrated, but these chemosensors may exhibit poor binding selectivity for Pb^{2+} over other heavy transition metal ions, which would reduce the accuracy of Pb^{2+} detection in practical applications. Hence, it is of interest to create highly sensitive and focused fluorescent chemosensors for naked-eye Pb^{2+} detection.[15,16]

Department of Chemistry, Guru Ghasidas Vishwavidyalaya, Bilaspur, C.G., India. E-mail: patra29in@yahoo.co.in; Tel: +91 7587312992

† Electronic supplementary information (ESI) available: Fig. S1–S10. See DOI: https://doi.org/10.1039/d3ra06185j

Azo compounds have been crucial as colorants because of their versatile application in diverse fields like electrophotography, laser printing, reversible optical storage, nonlinear optical devices, liquid crystalline displays, and biological-medical studies.[17,18] The wide range of applications for azo compounds, especially azobenzene dyes, can be attributed to their many benefits, including intense colour, simplicity in synthesis from inexpensive, easily accessible raw materials, desirable fastness properties, and special characteristics resulting from light-induced *cis–trans* isomerization.[19,20]

In continuation of our previous[21–25] studies in the search of fluorescent colorimetric Schiff bases, we report a novel, highly selective and sensitive optical chemosensor **L** based on triazole associated with azo dye for the easy onsite detection of Pb^{2+}. The introduction of SO_3H group into the flexible structure resulted in an improvement of the stability and the selectivity to metal ions as well as perfect solubility in aqueous solution. The presence of two donor sites and two acceptor sites increases the binding affinity of **L** and makes the detection limit lower than that of a single donor/acceptor (donor-π conjugation-acceptor) based chemosensor. The results showed that sensor **L** exhibited higher selectivity and sensitivity toward Pb^{2+} over many other metal ions in aqueous medium.

2. Experimental

2.1 General information

An X-4 digital melting-point device was used to determine the melting point, which was not corrected. Using a quartz cuvette with a 10 mm path length, UV-visible spectra were captured by a Shimadzu UV-vis 1800 spectrophotometer. A Hitachi spectrophotometer (RF-6000) was used to capture the fluorescence spectra. ^{1}H NMR and ^{13}C NMR spectra of the ligand were obtained with a Bruker Ultra Shield 400 MHz spectrometer, and the chemical shifts are given in ppm in relation to TMS. With a waters mass spectrometer, ESI-mass spectra were captured using a mixed solvent of HPLC methanol and triple-distilled water. All of the chemicals and metal salts were bought from Merck, and sodium was used as the counter ion for anions and nitrate for metals. In triple-distilled water, solutions of the receptor **L** (1×10^{-5} M) and metal salts (1×10^{-4} M) were made.

2.2 Synthesis of ligand L

The acidic $–SO_3H$ group of sulphanilic acid (1 mmol, 168 mg) was converted to $–SO_3Na$ group and its diazonium salt was prepared in good yield following previously described methods[26] with slight modification. After completion of the diazotization reaction, in another flask, salicylaldehyde (1 mmol, 122 mg) was dissolved in 10 mL water containing sodium hydroxide and sodium carbonate and cooled to 0 to −5 °C in an ice bath. The ice-cold diazonium solution was slowly added to the phenolate ion solution in basic medium by adjusting the pH at 7.5–8.5 over 30 min. The resulting solution was stirred for 30 min in an ice bath and then for 1 h at room temperature. The precipitate was collected and was washed several times with cold water after acidification of the solution (pH = 5.5–6.5) by addition of diluted HCl. The precipitate was finally re-crystallized from MeOH/H_2O to obtain the azo dye **1**.

A methanolic solution of the azo dye **1** (2 mmol in 25 mL) was added to another methanolic solution of 1*H*-1,2,4-triazole-3,5-diamine (0.099 g, 1 mmol in 25 mL). The reaction mixture was refluxed for 8 h, under dry condition. Then, it was slowly cooled to room temperature. A deep-red-coloured solid separated out, which was filtered off and dried in air. Yield: 0.612 g (75%); m.p. > 220 °C. Anal. found (calc. for $C_{28}H_{21}N_9O_8S_2$): C, 49.87 (49.77%); H, 3.08 (3.13%); N, 18.59 (18.66%). ESI-MS: 676.45 (MH^+, 25%) (Fig. S1†). FTIR/cm^{-1} (KBr): 1616 (*vs.*) (C=N), 1541 (*vs.*, N=N), 1483 (w), 1420 (w), 1363 (m), 1296 (s), 1198 (*vs.*, S=O), 1114 (s), 1042 (*vs.*), 998 (m), 900 (s), 834 (s), 755 (w), 708 (s), 638 (w) (Fig. S2†). ^{1}H NMR (400 MHz, $CDCl_3$, TMS): δ 11.62 (s, 1H, –NH), 10.68 (s, 2H, $–SO_3H$), 9.82 (s, 2H, –CH=N), 8.51 (s, 2H, phenyl), 7.98 (s, 4H), 7.52 (s, 2H, phenyl), 7.48 (m, 4H), 6.35 (m, 2H), 3.50 (s, 2H, –OH) (Fig. S3†). ^{13}C NMR (400 MHz, $CDCl_3$, TMS): δ 190.12, 160.07, 145.20, 139.62, 137.55, 132.15, 131.19, 130.26, 127.51, 129.39, 127.91, 126.46, 125, 32 (Fig. S4†). UV-visible: λ_{max}/nm (CH_3OH): 235 (11 200), 330 (17 500).

2.3 Preparation of stock solution for photophysical measurements

L (6.75 mg) was dissolved in 10 mL of triple-distilled water to make a solution of 1×10^{-3} M and 30 μL of this solution was diluted with 2.97 mL of solvent mixture to make a final concentration of 10 μM. The guest cation solutions were prepared separately using the corresponding nitrate salts at a concentration of 10 mM with triple-distilled water and further diluted to the desired concentration. After mixing **L** with each of the metal ions for a few seconds, UV-visible and fluorescence spectra were obtained at room temperature.

2.4 Job plot measurements

L (6.75 mg, 0.01 mmol) was dissolved in triple-distilled water (10 mL). 100, 90, 80, 70, 60, 50, 40, 30, 20, 10 and 0 μL of the **L** solution were taken and transferred to vials. Each vial was diluted with 2.9 mL of distilled water.

An aqueous solution of $Pb(NO_3)_2$ (10 μM) was prepared in triple-distilled water. 10, 20, 30, 40, 50, 60, 70, 80, 90 and 100 μL of the $Pb(NO_3)_2$ solution were added to each diluted **L** solution. Each vial had a total volume of 3 mL. After shaking them for a minute, absorption spectra were obtained at room temperature.

2.5 Competition with other metal ions

To determine the possible interference from other metal ions and selective binding affinity of chemosensor **L** towards Pb^{2+}, absorption spectra were obtained in the presence of other analytes. Chemosensor **L** (6.75 mg, 0.01 mmol) was dissolved in triple-distilled water (10 mL) and 30 μL of it was diluted to 3 mL to make a final concentration of 10 μM. $M(NO_3)_2$ (0.1 mmol) (where M = metal cation) was dissolved in 10 mL of triple-distilled water (each). 30 μL of each metal solution (10 mM, Al^{3+}, Hg^{2+}, Co^{2+}, Ni^{2+}, Zn^{2+}, Ca^{2+}, Mn^{2+}, Cd^{2+}, Cr^{3+}, Mg^{2+}, Fe^{3+} and Ag^+) was taken and added to 3 mL of the solution of receptor **L** (10 μM) to give 10 equiv. of metal ions. Then, 30 μL of metal solution (10 mM) was

added to the mixed solution of each metal ion and **L** to make 10 equiv. After mixing them for a few seconds, absorption spectra were obtained at room temperature.

2.6 pH study

This pH study has been considered as the charge separation of ligand with presence and absence of metal ion, the observed change was due to different absorbance behaviour of solution in the variation of pH. A set of buffer solutions with different range of pH values from 2 to 13 was prepared using 100 mM HEPES buffer. After the solution of desired pH was achieved, receptor **L** (6.75 mg) was dissolved in water (10 mL). For metal solution, 1 mM of $Pb(NO_3)_2$ was dissolved in HEPES buffer (10 mL, pH 7.00). 30 mL of these solutions (10 mM) was added to each of the previously made receptor solutions (10 M). After a brief period of mixing at room temperature, UV-visible spectra were obtained.

2.7 Computational details

The GAUSSIAN-09 revision C.01 program package was used for all calculations.[27] The gas-phase geometries of the compound were fully optimized without any symmetry restrictions in singlet ground state with the gradient-corrected density functional theory (DFT) level coupled with the hybrid exchange-correlation functional that uses Coulomb-attenuating method B3LYP.[28] Basis set 6-31++G was found to be suitable for the whole molecule. LanL2DZ basis sets were implemented for the geometry optimization of **L** + Pb^{2+} complex.

3. Results and discussion

3.1 Synthesis of ligand L

At the beginning, the starting material (*E*)-4-(3-formyl-4-hydroxyphenyl)diazyenyl benzenesulfonic acid (**1**) was synthesized by azo coupling reaction between salicylaldehyde and 4-aminobenzenesulfonic acid in good yield. This process was followed by the condensation reaction of 1*H*-1,2,4-triazole-3,5-diamine (trz) with the benzosulfonic azo dye to give rise to our desired chemosensor **L** which was precipitated out by methanol in pure state (Scheme 1). **L** was characterized by ^{1}H NMR, ^{13}C NMR, FT-IR and ESI-mass spectroscopy and elemental analysis.

In order to get the most probable structure of **L**, computations on the chemosensor **L** were performed based on DFT. The geometry-optimized structure and a schematic representation of the energy of MOs and contours of selected HOMO and LUMO orbitals of **L** are shown in Fig. 1. The calculated energy gap between HOMO and LUMO is 3.355 eV. The energy gap between HOMO and LUMO in the lead complex is 2.081 eV.

3.2 UV-visible spectral study of the chemosensor L

The optical behaviour of chemosensor **L** was investigated in water solution by using UV-visible absorption measurements. It was observed that initially the chemosensor **L** had a sharp single absorption band at 345 nm in aqueous solution which was attributed to the n–π^* transition.[29] After determining the optical properties of the newly synthesized triazole derivative **L**, the effect of other charged metal ions on its optical spectra was investigated. This absorption behaviour of **L** was almost constant for all selected metal ions Al^{3+}, Cu^{2+}, Cd^{2+}, Hg^{2+}, Zn^{2+}, Co^{2+}, Ni^{2+}, Mn^{2+}, Cr^{3+}, Fe^{3+} and Ag^{+} until addition of 3 equiv. of the different cations. This trend of similar spectra was changed for addition of Pb^{2+} ions. A blue-shifted absorption band appeared at 300 nm after addition of 2 equiv. of Pb^{2+} ions to the receptor solution with a clear observable colour change from yellow to colourless. More research was done on the ability of chemosensor **L** to detect metal ions. Fig. 2 illustrates **L** metal

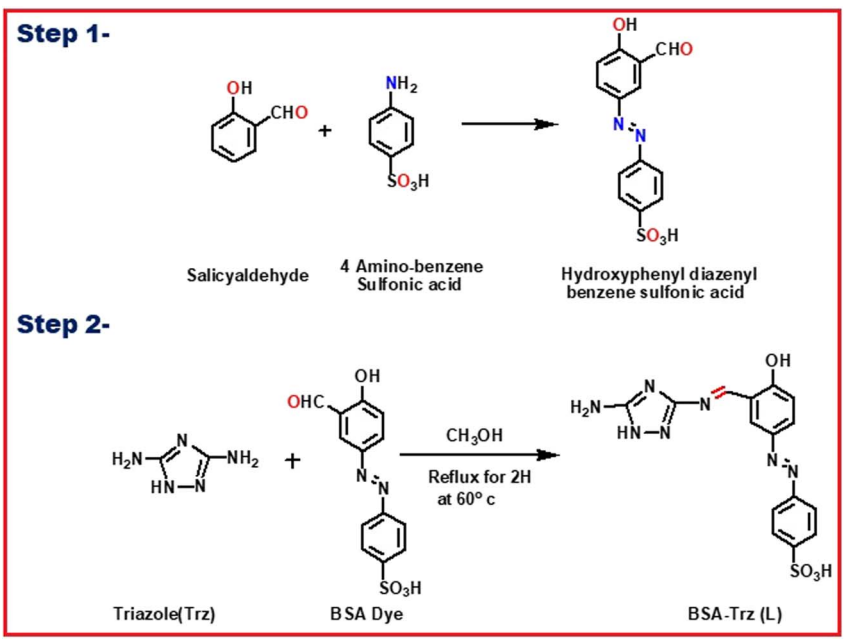

Scheme 1 Synthetic procedure of the probe L.

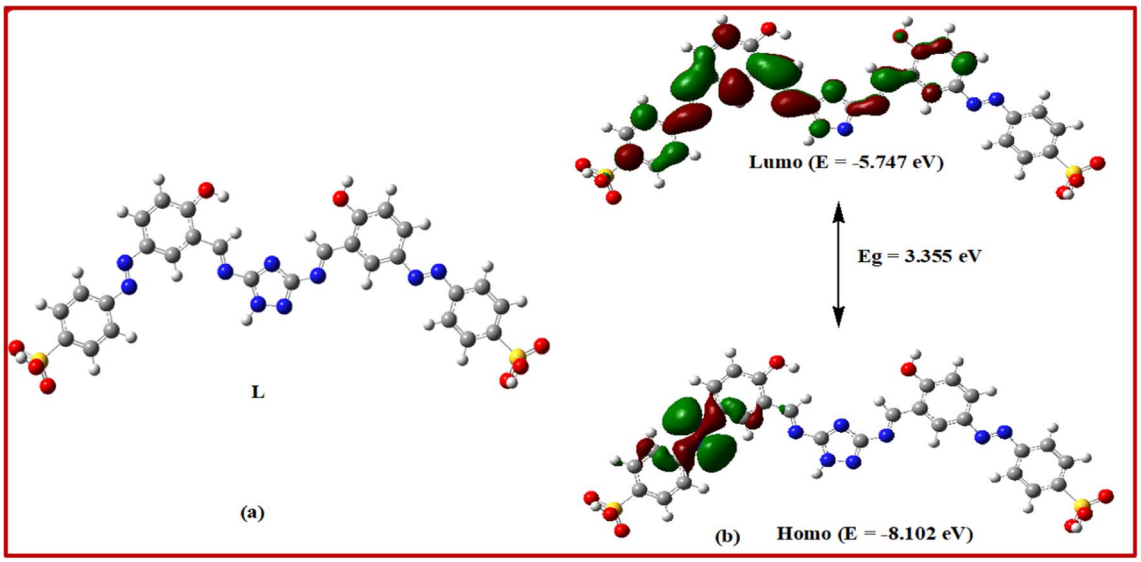

Fig. 1 (a) Optimized geometry and (b) frontier molecular orbitals and HOMO–LUMO energy gap of the probe L.

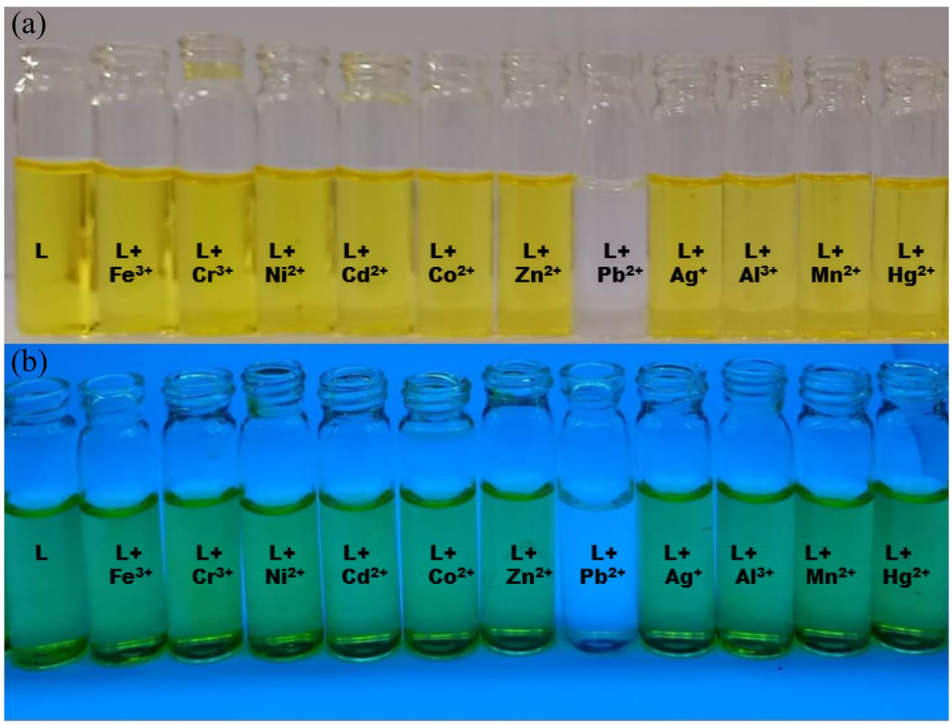

Fig. 2 Colour changes (a) to the naked eye and (b) under UV light of ligand L with Pb^{2+} ions and other cations in CH_3OH/H_2O (1 : 2).

ion selectivity; only Pb^{2+} creates a yellow to colourless transition that is visible to the unaided eye and when exposed to UV radiation (Fig. 3). No colour shift is caused by other metal ions. The colour changes were clearly visible to the naked eye and under UV light with Pb^{2+} in the presence of other metal ions.[30]

As expected from the above experimental analysis, we conclude that our synthesised **L** can be used for the selective detection of Pb^{2+} ions. We observed the best colorimetric and fluorometric response in a solvent mixture of MeOH : H_2O (1 : 2) when we examined the spectral behaviour of **L** with different types of solvent, *i.e.*, DMSO, ethanol, acetonitrile, water, MeOH : H_2O (1 : 1), MeOH : H_2O (1 : 2), the results of which are shown in Fig. 4 and Table 1.

Upon the addition of 2 equiv. of Pb^{2+} to **L**, the absorption band at 345 nm gradually decreased and a new absorption band appeared at 300 nm. A clear isosbestic point at 317 nm indicated the formation of only one complex species between **L** and Pb^{2+} (Fig. 5). The molar extinction coefficient of the new peak at

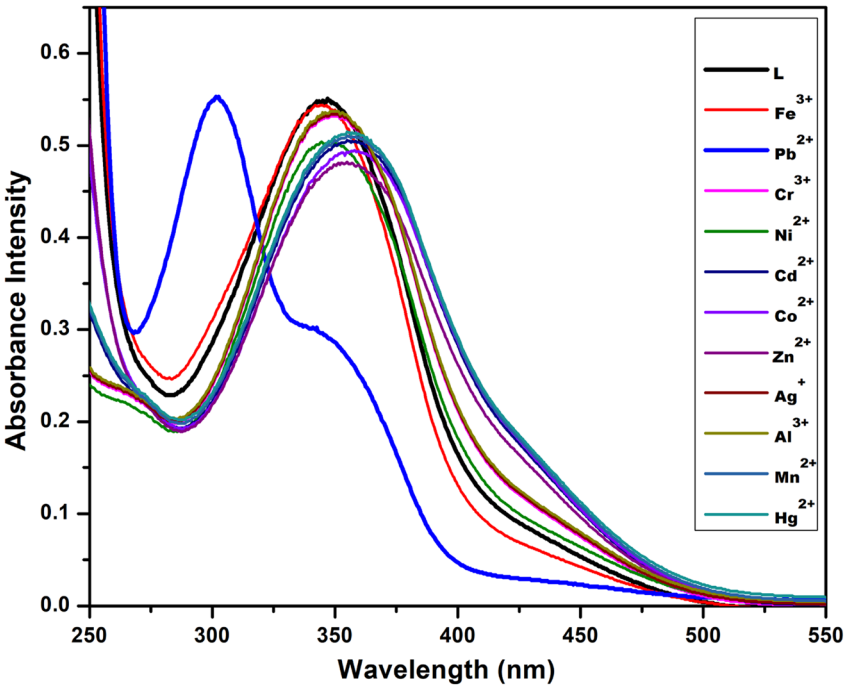

Fig. 3 Absorption spectra of L (10 μM) in the presence of 3 equiv. of different metal ions in $CH_3OH–H_2O$ (1 : 2).

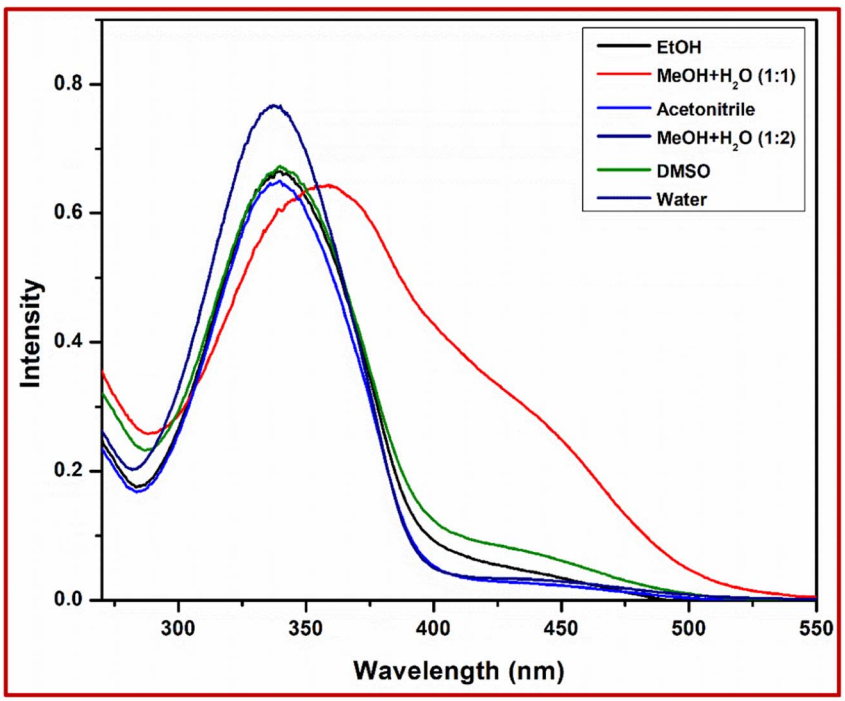

Fig. 4 Absorption spectra of L with different solvents and varied solvent concentration.

300 nm is 14.5×10^3 M^{-1} cm^{-1}, which is too large for Pb-based d–d transitions and thus must correspond to metal–ligand transitions. As there are blue shifts in the absorption spectra of Pb^{2+} with the chromophore **L**, there are chances for ligand to metal charge transfer (LMCT) and formation of a complex between the receptor **L** and Pb^{2+}. The colorimetric detection limit obtained from the titration curves was found to be 1.0×10^{-9} M for Pb^{2+} ions (Fig. 6), which is far below the WHO guidelines for drinking water. Thus, the chemosensor **L** can be applicable as a visual colorimetric probe towards Pb^{2+} at physiological conditions.

Table 1 Absorption properties of L in different solvents

Solvent	Absorption wavelength (nm)	log ε
DMSO	338	4.72
Acetonitrile	340	4.6
EtOH	337	4.79
MeOH : H_2O (1 : 1)	357	4.7
MeOH : H_2O (1 : 2)	345	4.88
Water	340	4.75

One of the important features of a chemosensor is its high selectivity towards metal ions and resistance to other interfering ions. To evaluate the selectivity of the receptor for the detection of Pb^{2+} ions, UV-visible spectra were obtained for the receptor **L** in the presence of a series of ions: Al^{3+}, Cu^{2+}, Cd^{2+}, Hg^{2+}, Zn^{2+}, Co^{2+}, Ni^{2+}, Mn^{2+}, Cr^{3+}, Fe^{3+} and Ag^{+} (Fig. 7). The intensity of the absorption band formed at 300 nm due to the formation of **L**–M^{2+} complex was not at all disturbed by the presence of other metal ions simultaneously in the solution. The colour intensity somewhat decreases only due to dilution effects. The other metals do not interfere with

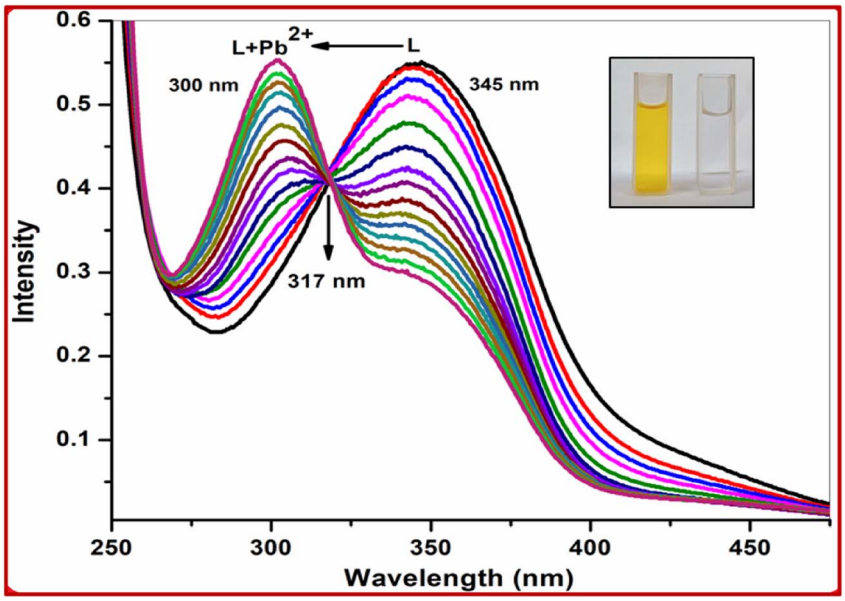

Fig. 5 UV-visible titration of L with Pb^{2+} in CH_3OH–H_2O (1 : 2). Inset: colour change of L on addition of 2 equiv. of Pb^{2+}.

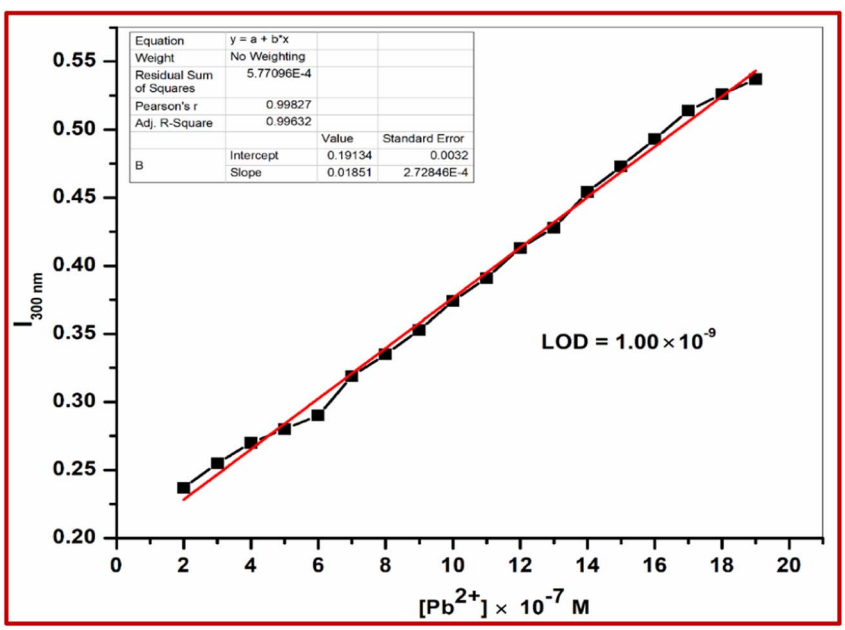

Fig. 6 Detection limit for Pb^{2+} from absorption spectra in CH_3OH–H_2O (1 : 2).

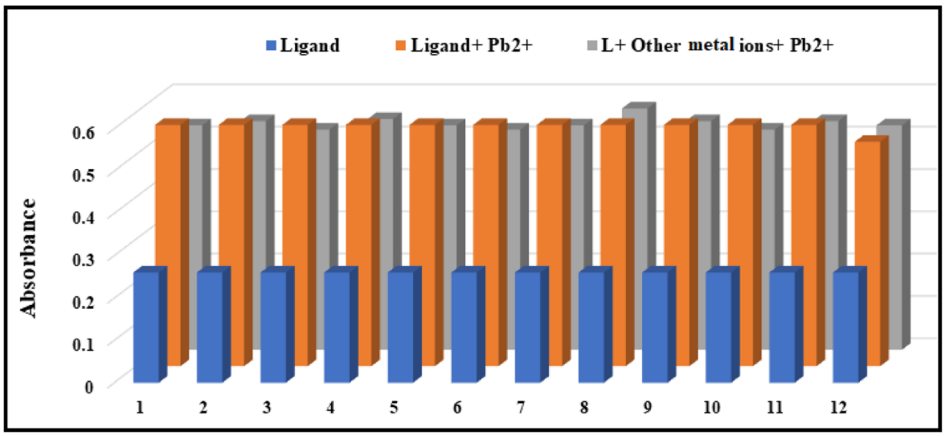

Fig. 7 Absorbance competitive experiment of L with other metal ions (where 1 = L, 2 = Fe^{3+}, 3 = Cr^{3+}, 4 = Ni^{2+}, 5 = Cd^{2+}, 6 = Ni^{2+}, 7 = Zn^{2+}, 8 = Pb^{2+}, 9 = Ag^{+}, 10 = Al^{3+}, 11 = Mn^{2+} and 12 = Hg^{2+}). Wavelength was monitored at 300 nm.

the fluorescence enhancement process. Thus, the predicted chemosensor **L** has selectivity towards Pb^{2+} ions even in the presence of 3-fold higher concentration of background ions.

3.3 Determination of stability constant

From UV-visible spectral changes, the binding constants for the formation of the respective complexes were evaluated using the Benesi–Hildebrand (B–H) plot, eqn (1):

$$\log\{(A - A_0)/(A_m - A)\} = n\log[M] + \log K \quad (1)$$

where A_0 is the absorbance of free **L** at a particular wavelength and A is the observed absorbance at that wavelength in any intermediate metal ion concentration (C). A_m is the absorption intensity value that was obtained in the presence of metal ion at saturation.

Assuming 1 : 2 interaction of **L** with Pb^{2+}, the binding constant (K) has been determined from the intercept of the linear plot (Fig. 8), which is found to be $K = 2.0 \times 10^7\ M^{1/2}$.

3.4 Stoichiometric measurements

Job's continuous variation method was used to determine the stoichiometry of the receptor for Pb^{2+} ions at a wavelength of 300 nm. The resulting curves showed a maximum at 0.62 mole fractions for Pb^{2+} ions indicating 1 : 2 complex formation between **L** and metal (Fig. S5†). In addition, the formation of the 1 : 2 complexations for **L**–Pb^{2+} was confirmed by ESI-mass spectrometry (Fig. 9). The positive-ion mass spectrum of **L** + Pb^{2+} showed

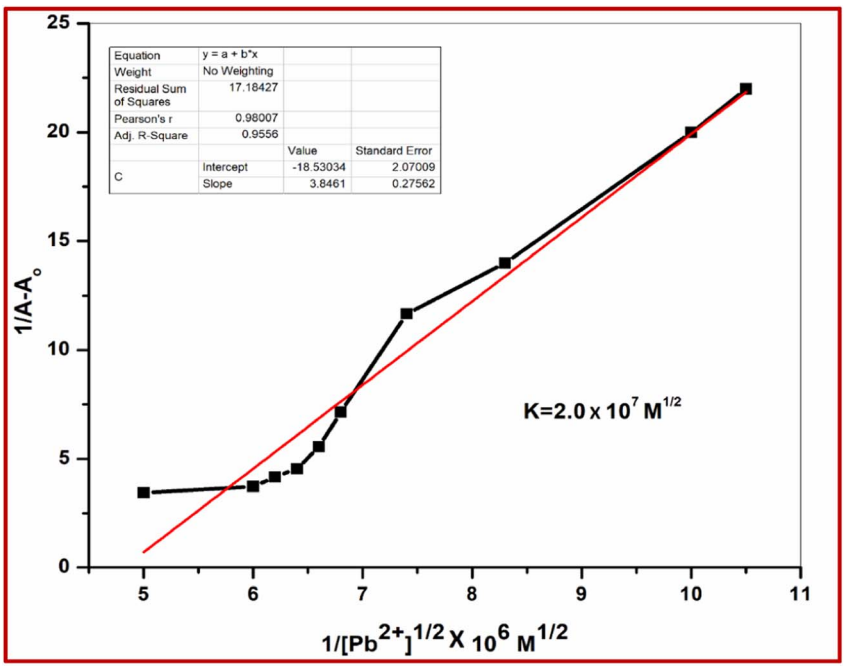

Fig. 8 Binding constants of L–Pb^{2+} complex.

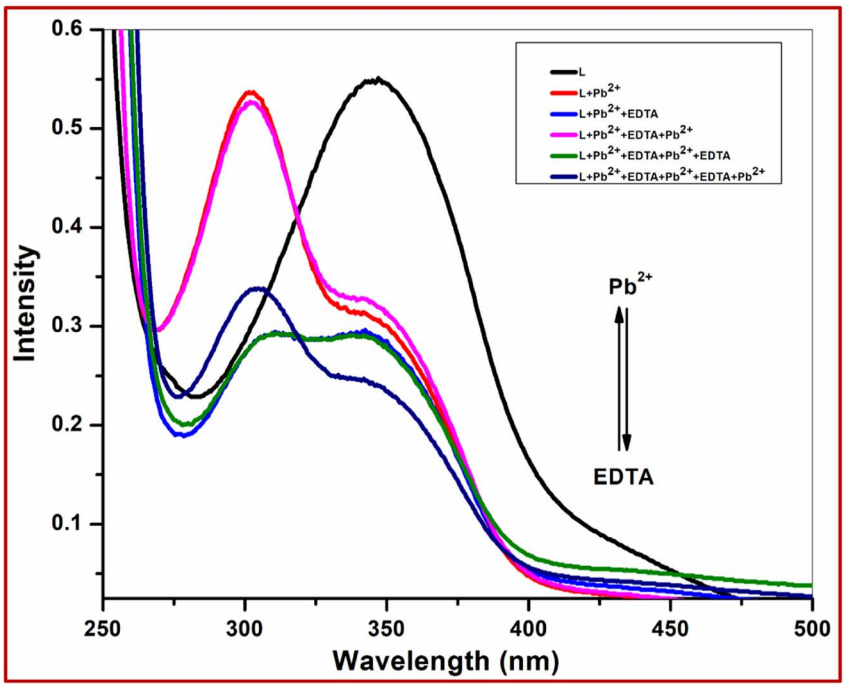

Fig. 9 Reversibility study of L complex with Na_2 EDTA.

that the peak at m/z = 1161.7595 was assignable to [**L** + $2Pb^{2+}$ + $4H_2O$] (Fig. S6†).

3.5 pH effect

The pH effects on the sensing process were also investigated, which showed that the chemosensor **L** is effective in a wide pH range from 6 to 13 for Pb^{2+} ion detection (Fig. S7†). At strongly acidic conditions (pH < 4) there exists a strong competition between H^+ ions and metal ions as well as the possibility of imine >C=N bond breaking, leading to inhibition of coordination ability. However, in basic solution (pH > 7) the absorption intensity of the **L**–Pb^{2+} complex around 300 nm was significantly lower as the un-protonated ionic substance can readily coordinate with Pb^{2+} ions.

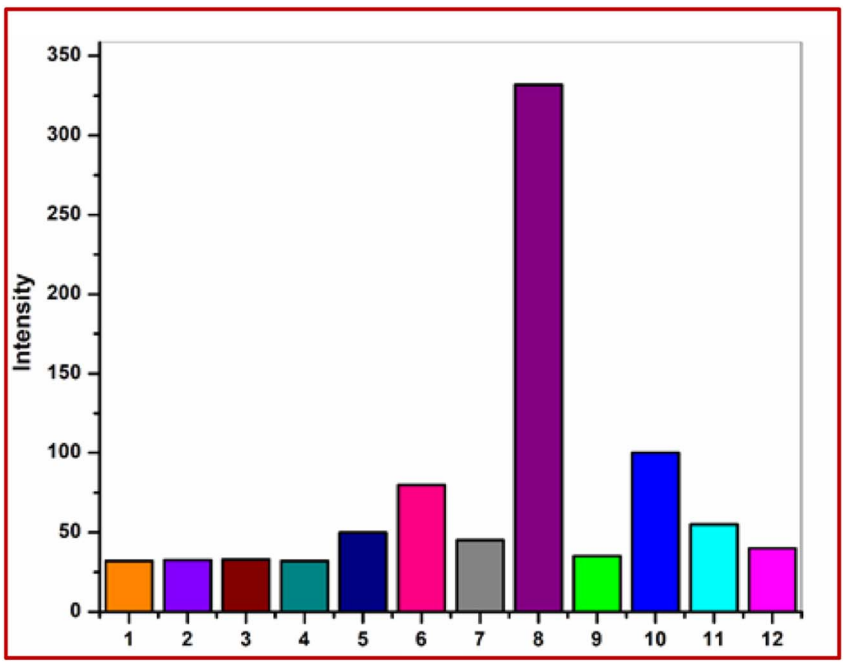

Fig. 10 Fluorescence study of L with different metal ions in CH_3OH–H_2O (1 : 2) on excitation at 310 nm and emission maxima at 417 nm (where 1 = L, 2 = Fe^{3+}, 3 = Cr^{3+}, 4 = Ni^{2+}, 5 = Cd^{2+}, 6 = Ni^{2+}, 7 = Zn^{2+}, 8 = Pb^{2+}, 9 = Ag^{+}, 10 = Al^{3+}, 11 = Mn^{2+} and 12 = Hg^{2+}).

3.6 Reversibility

The reversibility of chemosensor **L** has been investigated by using the common metal chelator disodium ethylenediaminetetraacetic acid (Na_2 EDTA). The absorption bands around 300 nm along with colourless solution of host–guest complex immediately turning yellow with the appearance of the original absorption band at 345 nm of **L** were observed when **L** + Pb^{2+} complex was treated with 2 equiv. of strong chelator Na_2EDTA (Fig. 9). With repeated addition of Pb^{2+} ions, the colour change and spectral change almost recovered. The switching behavior between **L** and **L** + Pb^{2+} complexes was systematic even after 3 cycles with the alternating addition of chelator and analyte (Fig. S8†).

3.7 Fluorescence studies of L toward different metal cations

The fluorescence behaviours of receptor **L** towards various metal ions (Al^{3+}, Cu^{2+}, Cd^{2+}, Hg^{2+}, Zn^{2+}, Co^{2+}, Ni^{2+}, Mn^{2+}, Cr^{3+}, Fe^{3+} and Ag^{+}) were investigated in methanol–water (1/2, v/v). Upon excitation at 310 nm at room temperature, **L** exhibits little emission at 417 nm with a low fluorescence quantum yield ($\Phi = 0.015$) with sky-blue coloration under a UV lamp. The low fluorescence intensity of **L** can be ascribed to the photoinduced electron transfer (PET) process and >C═N isomerization. However, the addition of nitrate salt of Pb^{2+} resulted in an immediate 8-fold enhancement of fluorescence intensity at 417 nm (Fig. 10). Other metal ions do not increase the fluorescence quantum yield. This is because of the fact that the presence of Pb^{2+} ions causes PET blocking through selective coordination to Pb^{2+} with the inner imino nitrogen atoms of the probe **L** (Scheme 2). In addition to the stable chelate formation of Pb^{2+} with **L**, the rigidity of the resulting complex is increased thereby generating efficient chelation-enhanced fluorescence.[30,31] These results clearly point to the receptor **L** being a selective sensor for Pb^{2+}.

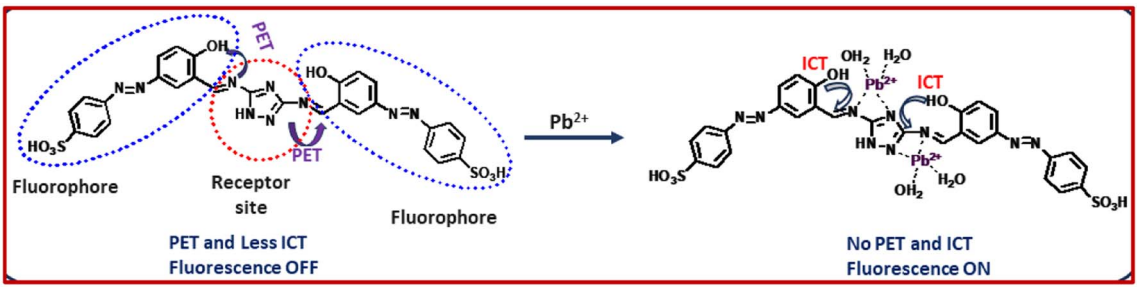

Scheme 2 Proposed sensing mechanism of L.

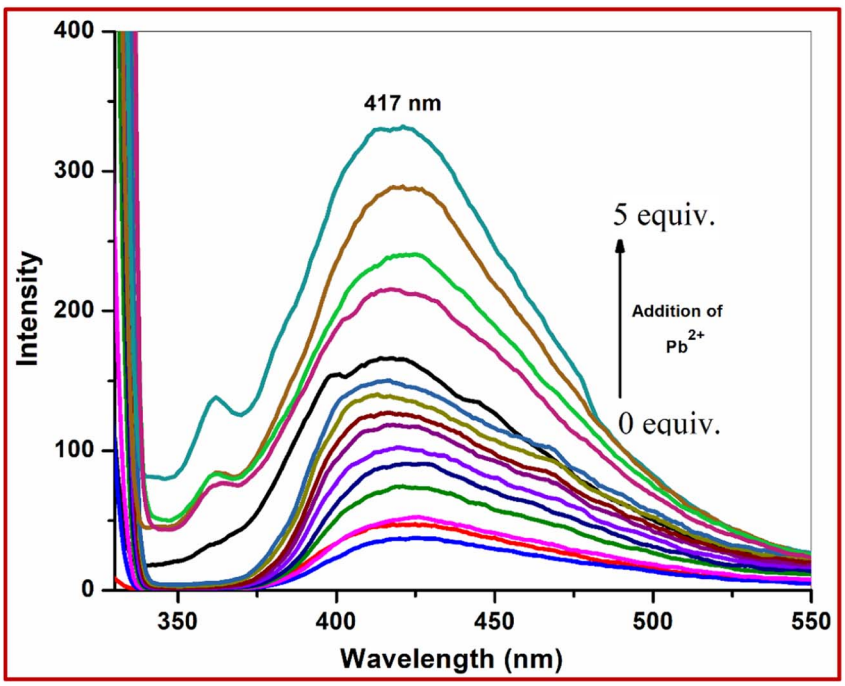

Fig. 11 Fluorescence titration of **L** with different concentrations of metal ions in CH_3OH–H_2O (1 : 2) on excitation at 310 nm.

3.8 Fluorescence titration

Sensitivity is an important criterion for the fluorescence sensor. To study the sensitivity of the receptor **L** with respect to Pb^{2+}, the probe **L** was titrated with Pb^{2+} ions. Upon gradual addition of Pb^{2+}, the fluorescence intensity increased gradually. The fluorescence changes of **L** upon addition of Pb^{2+} are shown in Fig. 11. From this titration profile it is observed that saturation is achieved after 4–5 equiv. addition of Pb^{2+} ions.

The fluorometric detection limit obtained from the titration curves was found to be 0.53×10^{-9} M for Pb^{2+} ions and the *R*-square value was 0.994 (Fig. 12). This detection limit was below the colorimetric detection limit. It is concluded that the fluorometric detection with the probe shows higher sensitivity. Thus, the chemosensor **L** can be applicable as a visual colorimetric and fluorometric probe towards Pb^{2+} at physiological conditions.

3.9 Fluorescence interference study

To examine the selectivity of the receptor **L** for the detection of Pb^{2+} ions, we measured the fluorescence spectra of the ligand **L**,

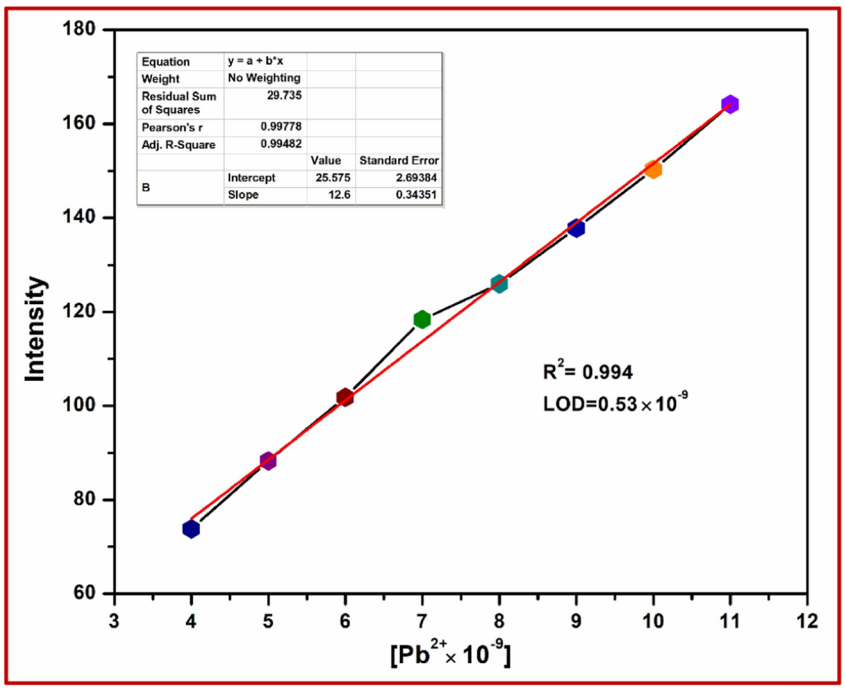

Fig. 12 Detection limit for Pb^{2+} from emission spectra in CH_3OH–H_2O (1 : 2).

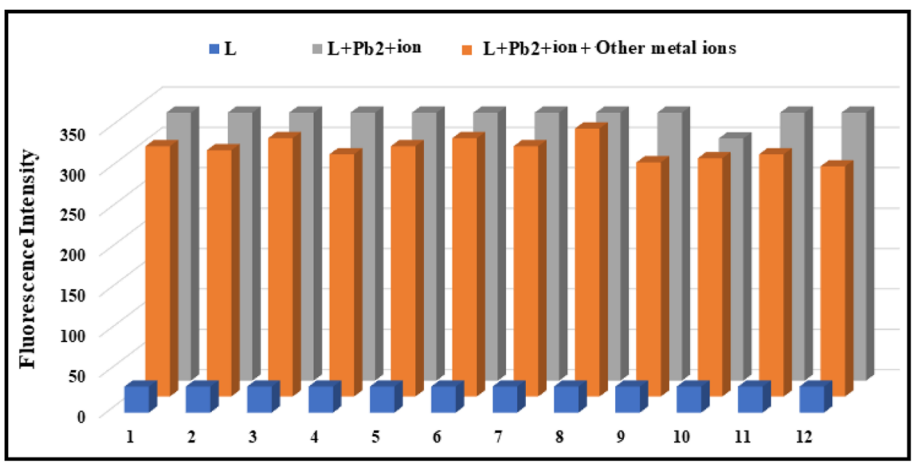

Fig. 13 Fluorescence interference study of L (where 1 = L, 2 = Fe^{3+}, 3 = Cr^{3+}, 4 = Ni^{2+}, 5 = Cd^{2+}, 6 = Ni^{2+}, 7 = Zn^{2+}, 8 = Pb^{2+}, 9 = Ag^{+}, 10 = Al^{3+}, 11 = Mn^{2+} and 12 = Hg^{2+}). Excitation wavelength was 340 nm and emission maxima were at 417 nm.

Table 2 Determination of Pb^{2+} ions in different water samples

Metal ion	Spiked amount (μM)	Recovered amount (μM)	% Recovery ± D ($n = 3$)
Pb^{2+}	5.00	5.06	101.6 ± 0.4
	10.00	9.97	99.7 ± 0.62
	20.00	19.95	98.2 ± 2.62

L + Pb^{2+} ions, and **L** + Pb^{2+} ions + other metal ions (Fig. 13) and observed that the fluorescence intensity of **L**–Pb^{2+} adduct is not altered in the presence of other metal ions.

3.10 Sensing mechanism of the probe L

The coordination sites of the proposed receptor towards selected guest Pb^{2+} were investigated by ^{1}H NMR spectral studies (Fig. S9†). The chemical shift at $\delta = 11.62$ ppm due to triazole –NH in free receptor **L** shifted upfield with the addition of 2 equiv. Pb^{2+} ions. Also, the azomethine proton signal shifted to the upfield region (from $\delta = 9.82$ ppm to $\delta = 9.1$ ppm), which confirmed the participation of imine in complexation. These upfield shifts are due to the chelation-induced internal charge transfer (ICT) process. This ^{1}H NMR behaviour of **L** was consistent even in the presence of 2-fold higher concentration of the analytes.

The FTIR spectra of **L** and its Pb(II) complexes are shown in Fig. S10.† The IR spectrum of free ligand **L** showed a broad band centred around 1616 cm^{-1} which is due to C=N groups of imine moiety and triazole. In the spectrum of the Pb^{2+} complex, these bands shifted towards lower wavenumbers to 1597 cm^{-1} which suggests that the azomethine group is involved in the coordination of both the metal ions to the ligand **L**. Further, the other peaks due to –NH and –CH groups of ligand **L** became small and shifted towards lower wavenumbers.

Metal sensing is primarily due to analyte recognition to binding site and signal transduction mechanism. The imine-attached triazole moiety contains multiple pockets suitable for metal coordination whereas the phenol containing two azine units act as a signalling sub-unit. Starting from absorption spectra, strong blue shift of absorption gives an indication for complexation at the acceptor site which enhances the ICT process in the ground state, allowing colorimetric sensing, and in the excited state both the PET and ICT effects were responsible for fluorometric sensing. The binding mechanism is shown in Scheme 2.

3.11 Real sample analysis

The chemosensor **L** was utilized successfully in the recognition of Pb^{2+} ions in different water samples. For this purpose, Pb^{2+} ion-contaminated samples were prepared individually through spiking different known concentration levels. Then, their concentrations were analysed with the sensing system described above. The experiment was repeated 3 times and a good recovery with very low standard deviation was observed. The results are presented in Table 2.

3.12 Analysis of biological samples by the chemosensor L

In order to check the potential of the chemosensor **L** for biological samples, the probe **L** of conc. 10 μM was successfully exploited for the recognition of Pb^{2+} in aqueous solution of bovine serum albumin (BSA) protein by fluorometry. Upon the addition of Pb^{2+}, the fluorescence intensity was increased in

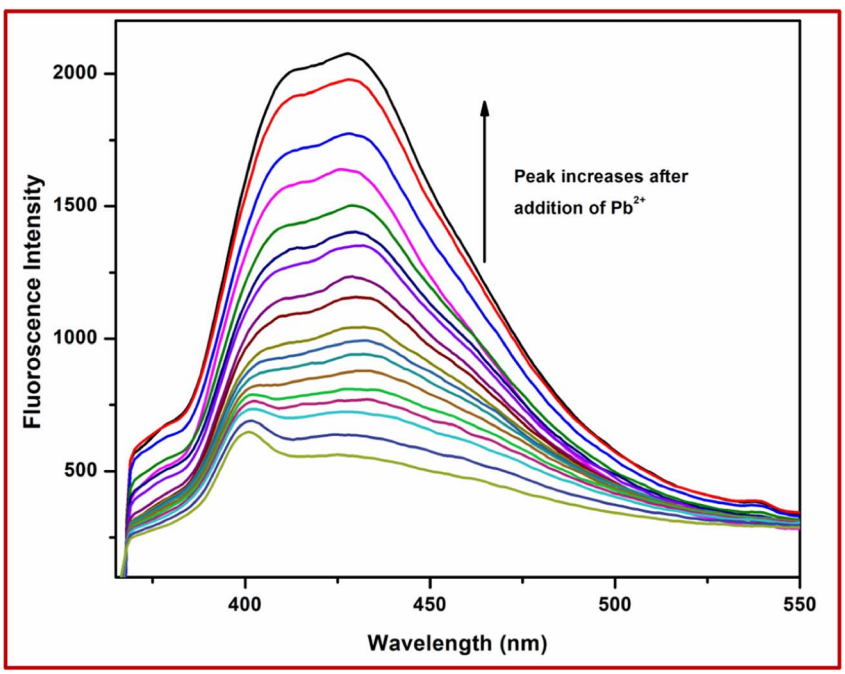

Fig. 14 Fluorescence spectra of **L** in the presence of 3 equiv. of Pb^{2+} in aqueous bovine serum albumin medium.

Table 3 Hydrogen bonding and molecular docking with centromere associated protein inhibitor protein targets

Protein (PDB ID)	No. of residues	Bond distance (Å)	Inhibition constant (micromolar)	Binding energy (kcal mol^{-1})	Reference RMSD (Å)
1USO	3	2.034 2.182 1.994 2.175 2.334	0.0031	−11.6	24.591

BSA medium. An almost one-hundredth increase in emission intensity was observed in the case of Pb^{2+} (Fig. 14).

3.13 Molecular docking studies

Triazole derivatives possess a wide range of biological properties like antioxidant, anti-inflammatory, antibacterial, antiviral, antimalarial, *etc.* Molecular docking studies were carried out to reveal the biological properties and binding mode at the active site of proteins. In order to find the best position to dock our ligand[32] **L**, we first used Swiss ADME target prediction utilising a database from the protein database (RCSB PDB). After that, we used Chimera 1.14 to minimise the structure.[33] The probe **L** had no trouble docking with the oxidoreductase protein 1USO. The lowest binding energy, −11.6 kcal mol^{-1}, indicates that this is biologically active. The bound residue of 1USO and the ligand are separated by hydrogen bonds with distances of 2.034, 2.182, 1.994, 2.175 and 2.334 Å. The molecule shows strong bioactivity as concluded from its low binding energy score. Finding the H-bond distance between the residue and the ligand (compound) shows that this ligand is appropriate for use with a protein receptor (Table 3).[34] Different interactions in 2D molecular docking diagrams (using Discovery studio tool) are clearly demonstrated in Fig. 15.

3.14 Comparison of L with other previously reported chemosensors for Pb^{2+} ions

As part of our ongoing effort for providing useful analytical techniques to monitor the increasing number of analytes of environmental relevance as quickly and as cheaply as possible and with the highest sensitivity, the present paper describes the

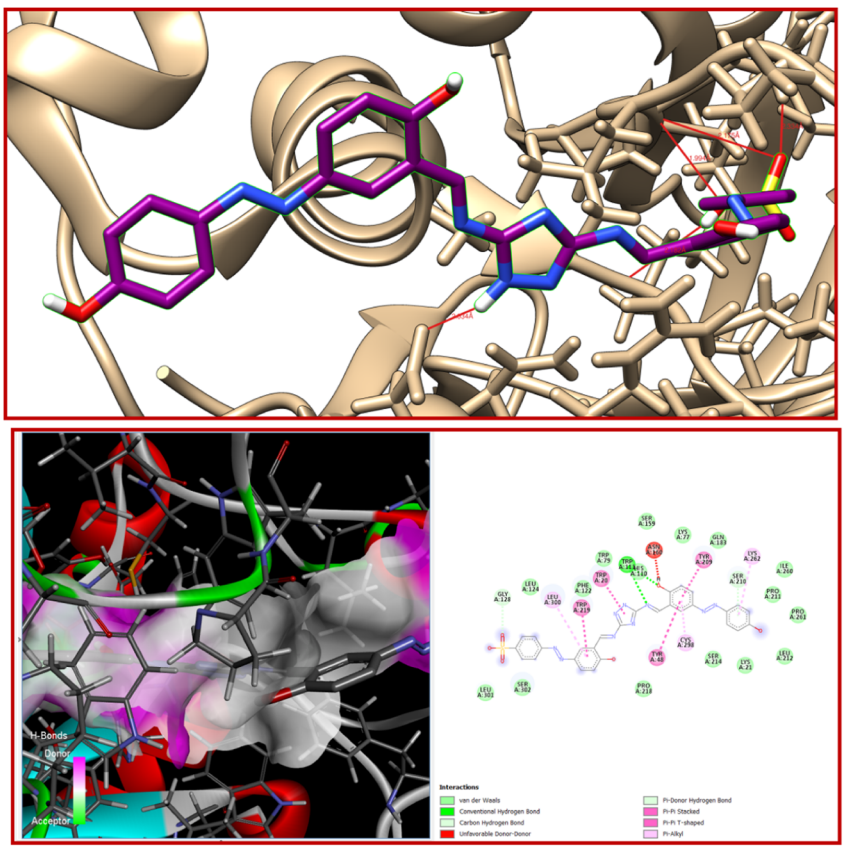

Fig. 15 Interaction of L with oxidoreductase protein 1USO.

Table 4 Comparison of some previously reported chemosensors for Pb^{2+} ions

Structure of probe	Solvent/medium	Sensing method	Binding constant	LOD	Ref.
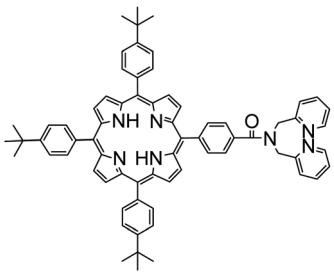	CH_2Cl_2–MeOH (1 : 1)	Both colorimetric and fluorescent	2.1×10^4	3.1×10^{-7} M for Pb^{2+}	35
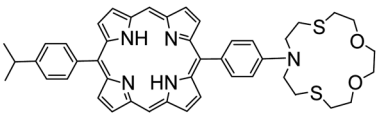	CH_2Cl_2–MeOH (3 : 2)	Both chromogenic and fluorogenic	3.4×10^4	2.6×10^{-13} M for Cu^{2+} 1.3×10^{-11} M for Pb^{2+}	36
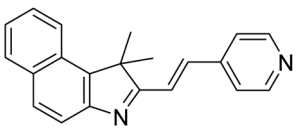	CH_3CN–water mixture (9 : 1, v/v)	Fluorescent sensor	Not available	1.24 μM for Cu^{2+} 3.41 μM for Pb^{2+}	37
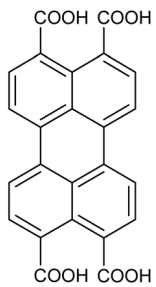	Aqueous solution	Both colorimetric and fluorescent	Not available	Not available	38
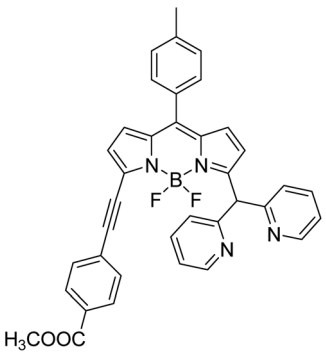	CH_3CN	Colorimetric and fluorescent chemosensor	5.01×10^5	0.14 μM	39
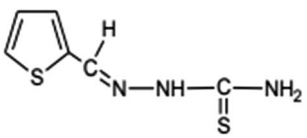	PVC : DOP:LL2 : NaTPB	Potentiometric		1.0×10^{-7} M	40
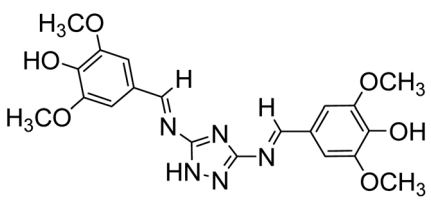	CH_3OH-tris buffer (1 : 1, v/v)	Colorimetric and fluorescent chemosensor	9×10^5	Colorimetric: 1.2×10^{-6}; fluorometric: 9×10^{-7} M	41

Table 4 (*Contd.*)

Structure of probe	Solvent/medium	Sensing method	Binding constant	LOD	Ref.
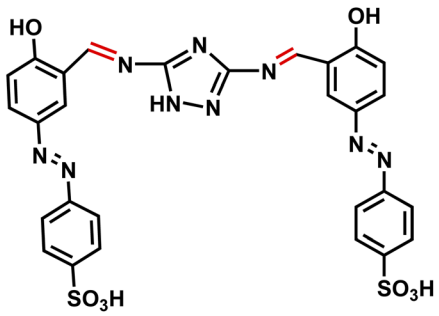	MeOH–H_2O	Colorimetric and fluorescent chemosensor	2×10^7	Colorimetric: 1.0×10^{-9} M; fluorometric: 0.53×10^{-9} M	Present work

synthesis of a new fluorescent-colorimetric probe **L**, which was validated for detection and quantification of Pb^{2+} ions in aqueous–methanol medium.

There are several reports where a few Schiff base, macrocyclic and bodipy compounds have been utilized for the selective detection of Pb^{2+} ions. The probe **L** was compared with those reported chemosensors (Table 4). While each of the other chemosensors showed some advantages such as high sensitivity and selectivity, the important features of the fluorescent-colorimetric chemosensor **L** are easy, practical and cost-effective synthesis and naked-eye detection as well as high sensitivity and selectivity.

4. Conclusion

Herein, we report a perfectly water soluble novel bis-Schiff base simple colorimetric and turn-on fluorescence chemosensor **L** with a triazole moiety for the sensitive and selective detection of Pb^{2+} in CH_3OH–water (1 : 2, v/v). In the presence of Pb^{2+} ions, **L** displayed good fluorescence characteristics with discernible colour change from yellow to colourless. To the best of our knowledge, there are several papers concerning fluorescence-enhanced probes for triazole-based cations, but only a few concerning reversible "off–on" fluorescent probes for the triazole-based detection of Pb^{2+} ions. Additionally, ^{1}H-NMR, FTIR, and ESI-mass spectrometry were used to explore the sensing mechanism. The colorimetric detection limit for Pb^{2+} is 1.0×10^{-9} M. The chemosensor **L** shows its application potential in the detection of Pb^{2+} in BSA proteins and in real samples. Moreover, we have studied the molecular docking of the probe **L**.

Author contributions

Vanshika Sharma: conceptualization, methodology, investigation, formal analysis, visualization and writing – original draft. Sandhya Savita: theoretical calculations. Dr Goutam Kumar Patra: conceptualization, review, editing, funding acquisition and supervision.

Conflicts of interest

The authors declare no conflicts of interest.

Acknowledgements

G. K. P. would like to thank the Department of Science and Technology (SR/FST/CSI-264/2014 and EMR/2017/0001789) and Department of Biotechnology, Government of India, New Delhi for financial support.

References

1 M. H. Mashhadizadeh, M. Pesteh, M. Talakesh, I. Sheikhshoaie, M. M. Ardakani and M. A. Karimi, *Spectrochim. Acta, Part B*, 2008, **63**, 885–888.
2 C. F. Harrington, S. A. Merson and T. M. D. D'Silva, *Anal. Chim. Acta*, 2004, **505**, 247–254.
3 S. L. C. Ferreira, A. S. Queiroz, M. S. Fernandes and H. C. dos Santos, *Spectrochim. Acta, Part B*, 2002, **57**, 1939–1950.
4 R. N. Goyal, V. K. Gupta and S. Chatterjee, *Sens. Actuators, B*, 2010, **149**, 252–258.
5 R. Kumar, V. Bhalla and M. Kumar, *Dalton Trans.*, 2013, **42**, 8808–8814.
6 (*a*) Y. Li and A. H. Flood, *Angew. Chem., Int. Ed.*, 2008, **47**, 2649–2652; (*b*) Y. Li and A. H. Flood, *J. Am. Chem. Soc.*, 2008, **130**, 12111–12122.
7 D. Wang, J. Q. Zheng, X. Yan, X. J. Zheng and L. P. Jin, *RSC Adv.*, 2015, **5**, 64756–64762.
8 J. Liu, M. Yu, X. C. Wang and Z. Zhang, *Spectrochim. Acta*, 2012, **A93**, 245–249.
9 X. Zhou, S. Lee, Z. Xu and J. Yoon, *Chem. Rev.*, 2015, **115**, 7944–8000.
10 A. K. Manna, M. Sahu, K. Rout, U. K. Das and G. K. Patra, *Microchem. J.*, 2020, **157**, 104860.
11 Y. Erel, T. Axelrod, A. Veron, Y. Mahrer, P. Katsafados and U. Dayan, *Environ. Sci. Technol.*, 2002, **36**, 3230.
12 (*a*) C. B. Swearingen, D. Wernette, P. D. M. Cropek, Y. Lu, J. V. Sweedler and P. W. Bohn, *Anal. Chem.*, 2005, **77**, 442;

(*b*) J. Li and Y. Lu, *J. Am. Chem. Soc.*, 2000, **122**, 10466; (*c*) D. W. Domaille, E. L. Que and C. J. Chang, *Nat. Chem. Biol.*, 2008, **4**, 168.

13 L. Bonin, V. Vitry and F. Delaunois, *Sustainable Mater. Technol.*, 2020, **23**, e00130.

14 L. D. Grant, Lead and compounds, in *Environmental Toxicants: Human Exposures and Their Health Effects*, 2020, pp. 627–675.

15 (*a*) Y. Xiao, A. A. Rowe and K. W. Plaxco, *J. Am. Chem. Soc.*, 2007, **129**, 262; (*b*) F. Chai, C. Wang, T. Wang, L. Li and Z. Su, *ACS Appl. Mater. Interfaces*, 2010, **2**, 1466.

16 A. Ghorai, J. Mondal, R. Saha, S. Bhattcharya and G. K. Patra, *Anal. Methods*, 2016, **8**, 2032–2040.

17 J. K. Fawell, *Guidelines for Drinking Water Quality*, World Organization, Geneva, 2nd edn, 1996, vol. 2, pp. 940–1033.

18 S. Menati, A. Azadbakht, R. Azadbakht, A. Taeb and A. Kakanejadifard, *Dyes Pigm.*, 2013, **98**, 499–506.

19 A. Mohammadi, Z. Dehghana, M. Rassa and N. Chaibakhsh, *Sens. Actuators, B*, 2016, **230**, 388–397.

20 A. K. Manna, J. Mondal, R. Chandra, K. Rout and G. K. Patra, *Anal. Methods*, 2018, **10**, 2317.

21 M. Sahu, A. K. Manna and S. Chowdhaury, *RSC Adv.*, 2020, **10**, 44860.

22 M. Sahu, A. K. Manna and G. K. Patra, *Mater. Adv.*, 2022, **3**, 2495.

23 V. Sharma, M. Sahu, A. K. Manna, D. De and G. K. Patra, *RSC Adv.*, 2022, **12**, 34226–34235.

24 A. Ghorai, J. Mondal, A. K. Manna, S. Chowdhury and G. K. Patra, *Anal. Methods*, 2018, **10**, 1063–1073.

25 A. Ghorai, J. Mondal and G. K. Patra, *J. Mol. Struct.*, 2015, **1097**, 52–60.

26 A. Mohammadi, M. R. Yazdanbakhsh and L. Farahnak, *Spectrochim. Acta, A*, 2012, **89**, 238.

27 M. J. Frisch, G. W. Trucks, H. B. Schlegel, G. E. Scuseria, M. A. Robb, J. R. Cheeseman, G. Scalmani, V. Barone, B. Mennucci, G. A. Petersson, H. Nakatsuji, M. Caricato, X. Li, H. P. Hratchian, A. F. Izmaylov, J. Bloino, G. Zheng, J. L. Sonnenberg, M. Hada, M. Ehara, K. Toyota, R. Fukuda, J. Hasegawa, M. Ishida, T. Nakajima, Y. Honda, O. Kitao, H. Nakai, T. Vreven, J. A. Montgomery Jr, J. E. Peralta, F. Ogliaro, M. Bearpark, J. J. Heyd, E. Brothers, K. N. Kudin, V. N. Staroverov, R. Kobayashi, J. Normand, K. Raghavachari, A. Rendel, J. C. Burant, S. S. Iyengar, J. Tomasi, M. Cossi, N. Rega, J. M. Millam, M. Klene, J. E. Knox, J. B. Cross, V. Bakken, C. Adamo, J. Jaramillo, R. Gomperts, R. E. Stratmann, O. Yazyev, A. J. Austin, R. Cammi, C. Pomelli, J. W. Ochterski, R. L. Martin, K. Morokuma, V. G. Zakrzewski, G. A. Voth, P. Salvador, J. J. Dannenberg., S. Dapprich, A. D. Daniels, Ö. Farkas, J. B. Foresman, J. V. Ortiz, J. Cioslowski and D. J. Fox, *Gaussian 09, Revision C.01*, Gaussian Inc., Wallingford, CT, 2009.

28 (*a*) A. D. Becke, *J. Chem. Phys.*, 1993, **98**, 5648; (*b*) C. Lee, W. Yang and R. G. Parr, *Phys. Rev. B: Condens. Matter Mater. Phys.*, 1988, **37**, 785.

29 A. K. Manna, J. Mondal, K. Rout and G. K. Patra, *Sens. Actuators, B*, 2018, **275**, 350–358.

30 P. Venkatesan, N. Thirumalivasan and S. P. Wu, *RSC Adv.*, 2017, **7**, 21733–21739.

31 V. Sharma, B. Sahu, U. K. Das and G. K. Patra, *Inorg. Chim. Acta*, 2023, **552**, 121491.

32 S. Savita, A. Fatima, K. Garima, K. Pooja, I. Verma, N. Siddiqui and S. Javed, *J. Mol. Struct.*, 2021, **1243**, 130932.

33 E. F. Pettersen, T. D. Goddard, C. C. Huang, G. S. Couch, D. M. greenblatt, E. C. meng and T. E. Ferrin, *J. Com. Chem.*, 2004, **25**, 1605–1612.

34 N. Singh, A. Fatima, M. Singh, M. Kumar, I. Verma, S. Muthu, N. Siddiqui and S. Javed, *J. Mol. Liquids*, 2022, **351**, 118670.

35 Y. Chen and J. Jiang, *Org. Biomol. Chem.*, 2012, **10**, 4782.

36 Y. Chen and K. Wang, *Photochem. Photobiol. Sci.*, 2013, **12**, 2001.

37 X. Yang, W. Zeng, L. Wang, X. Lu, Y. Yan, J. Qu and R. Liu, *RSC Adv.*, 2014, **4**, 22613.

38 S. Sowmiyha, V. Kumar, J. Pitchaimani, V. Madhu, R. Thiagarajan, N. S. Subramanian and S. P. Anthony, *J. Lumin.*, 2018, **203**, 42.

39 Z. Gu, H. Cheng, X. Shen, T. He, K. Jiang, H. Qiu, Q. Zhang and S. Yin, *Spectrochim. Acta, Part A*, 2018, **203**, 315.

40 C. Mohan, K. Sharma and S. Chandra, *Anal. Bioanal. Electrochem.*, 2022, **14**, 860–870.

41 K. Rout, A. K. Manna, M. Sahu, J. Mondal, S. K. Singh and G. K. Patra, *RSC Adv.*, 2019, **9**, 25919–25931.